

# Imprints of $CP$ violation induced by sterile neutrinos in T2K data

N. Klop\* and A. Palazzo

*Max-Planck-Institut für Physik (Werner Heisenberg Institut), Föhringer Ring 6, 80805 München, Germany*

We investigate the impact of light ( $\sim$  eV) sterile neutrinos in the long-baseline experiment T2K. We show that, within the 3+1 scheme, for mass-mixing parameters suggested by the short-baseline anomalies, the interference among the sterile and the atmospheric oscillation frequencies induces a new term in the  $\nu_\mu \rightarrow \nu_e$  transition probability, which has the same order of magnitude of the standard 3-flavor solar-atmospheric interference term. We show, for the first time, that current T2K data, taken together with the results of the  $\theta_{13}$ -dedicated reactor experiments, are sensitive to two of the three  $CP$ -violating phases involved in the 3+1 scheme. Both the standard  $CP$ -phase and the new one ( $\delta_{13} \equiv \delta$  and  $\delta_{14}$  in our parameterization choice) tend to have a common best-fit value  $\delta_{13} \simeq \delta_{14} \simeq -\pi/2$ . Quite intriguingly, the inclusion of sterile neutrino effects leads to better agreement between the two estimates of  $\theta_{13}$  obtained, respectively, from reactors and T2K, which in the 3-flavor framework are slightly different.

PACS numbers: 14.60.Pq, 14.60.St

## I. INTRODUCTION

Neutrino physics is entering a new era. The discovery of a relatively large value of the long-sought third mixing angle  $\theta_{13}$  has raised hopes of completing the picture of the standard 3-flavor framework. The determination of the two missing unknown properties, i.e., the amount (if any) of leptonic  $CP$ -violation (CPV) and the neutrino mass hierarchy (NMH) are now realistic targets.

Leptonic CPV is a genuine 3-flavor phenomenon [1], which can occur only if no pair of neutrino mass eigenstates is degenerate ( $m_i^2 - m_j^2 \neq 0$  for  $i \neq j$ ,  $i, j = 1, 2, 3$ ) and if all the three mixing angles ( $\theta_{12}, \theta_{23}, \theta_{13}$ ) are nonzero. Now that all these (six) necessary conditions are known to be realized in nature, the next task is to ascertain if a further (last) condition is fulfilled, i.e., if the lepton mixing matrix is non-real, or, equivalently, if the  $CP$ -phase  $\delta$  is different from 0 and  $\pi$ . The  $CP$ -phase  $\delta$  is already being probed by the long-baseline (LBL) accelerator experiment T2K [2] (and also by MINOS [3] with less statistical power) in combination with the reactor  $\theta_{13}$ -dedicated experiments [4–7], which “fix”  $\theta_{13}$  independently of  $\delta$ . Some (weaker) information on such a fundamental phase is also provided by atmospheric neutrinos [8]. Quite intriguingly, all the latest global analyses [9–11] show a weak indication (close to the 90% C.L.) of CPV, the best-fit value of the  $CP$ -phase being  $\delta \sim -\pi/2$ .

An apparently unrelated issue in present-day neutrino physics is provided by the hints of light ( $\sim$  eV) sterile species suggested by the short-baseline (SBL) anomalies (see [12–14] for reviews). In the presence of sterile neutrinos, the 3-flavor scheme must be enlarged so as to include one (or more) mass eigenstates having nonzero admixture with the active flavors. In such more general

frameworks, new  $CP$ -phases automatically appear and, thus, the question naturally arises as to whether the current and planned LBL experiments, designed to underpin the standard  $CP$ -phase  $\delta$ , also have some chance to detect the new potential sources of CPV.<sup>1</sup>

In this work we show, for the first time, that the existing measurements of  $\nu_\mu \rightarrow \nu_e$  appearance performed by the LBL experiment T2K, taken in combination with those of  $\bar{\nu}_e \rightarrow \bar{\nu}_e$  disappearance deriving from the  $\theta_{13}$ -dedicated reactor experiments, are *already* able to provide information on the nonstandard sterile-induced  $CP$  phases. In fact, differently from the SBL experiments, in LBL setups the oscillations induced by the new sterile neutrino species can interfere with those driven by the two standard squared-mass splittings giving rise to observable effects. In particular, it turns out that the interference among the sterile and the atmospheric oscillation frequencies induces a new term in the  $\nu_\mu \rightarrow \nu_e$  transition probability, which has the same order of magnitude of the standard 3-flavor solar-atmospheric interference term.

Working within the simple 3+1 scheme, we show that, for mass-mixing parameters suggested by the current SBL fits [13, 14], it is possible to extract quantitative information on two of the three  $CP$  phases involved in the model (one of them being the standard phase  $\delta$ ). Quite intriguingly, the statistical significance of the information obtained on the new  $CP$  phase is similar to that achieved for the standard phase  $\delta$ . In addition, our analysis evidences that the presence of 4-flavor effects tends to resolve the slight tension (present within the 3-flavor framework) between the two estimates of  $\theta_{13}$  extracted, respectively, from T2K and from reactor experiments.

The rest of the paper is organized as follows. In Sec. II we introduce the theoretical framework needed to discuss the analytical behavior of the LBL  $\nu_\mu \rightarrow \nu_e$  transition

---

\*Now at GRAPPA Institute, University of Amsterdam, Science Park 904, 1098 XH Amsterdam, Netherlands

---

<sup>1</sup> Previous work on the effects of light sterile neutrinos in LBL setups can be found in [15–24].

probability in vacuum. In Sec. III we present the results of the numerical analysis (which includes the matter effects). In Sec. IV we draw our conclusions. The paper is closed by an appendix dedicated to the analytical treatment of the MSW effects relevant for the LBL setups within the 3+1 scheme.

## II. THEORETICAL FRAMEWORK

Light sterile neutrinos are introduced in the so-called  $3 + N_s$  schemes, where the  $N_s$  new mass eigenstates are assumed to be separated from the three standard ones by large splittings, giving rise to the hierarchal pattern  $\Delta m_{12}^2 \ll |\Delta m_{13}^2| \ll |\Delta m_{1k}^2|$  ( $k = 4, \dots, 3 + N_s$ ), with  $\Delta m_{ij}^2 \equiv m_j^2 - m_i^2$ . This implies that the fast oscillations induced by the new squared-mass splittings are completely averaged in all setups sensitive to the solar squared-mass difference ( $\Delta m_{12}^2$ ) and the atmospheric one ( $\Delta m_{13}^2$ ). In this work, for definiteness, we consider the simplest 3+1 scheme.

In the presence of a fourth sterile neutrino  $\nu_s$ , the flavor ( $\nu_\alpha$ ,  $\alpha = e, \mu, \tau, s$ ) and the mass eigenstates ( $\nu_i$ ,  $i = 1, 2, 3, 4$ ) are connected through a  $4 \times 4$  unitary mixing matrix  $U$ , which depends on six complex parameters [25]. Such a matrix can be expressed as the product of six complex elementary rotations, which define six real mixing angles and six  $CP$ -violating phases. Of the six phases three are of the Majorana type and are unobservable in oscillation processes, while the three remaining ones are of the Dirac type. As it will appear clear in what follows, for the treatment of the transitions involved in LBL setups, a particularly convenient choice of the parameterization of the mixing matrix is<sup>2</sup>

$$U = \tilde{R}_{34} R_{24} \tilde{R}_{14} R_{23} \tilde{R}_{13} R_{12} \quad (1)$$

where  $R_{ij}$  ( $\tilde{R}_{ij}$ ) represents a real (complex)  $4 \times 4$  rotation in the  $(i, j)$  plane containing the  $2 \times 2$  submatrix

$$R_{ij}^{2 \times 2} = \begin{pmatrix} c_{ij} & s_{ij} \\ -s_{ij} & c_{ij} \end{pmatrix} \quad \tilde{R}_{ij}^{2 \times 2} = \begin{pmatrix} c_{ij} & \tilde{s}_{ij} \\ -\tilde{s}_{ij}^* & c_{ij} \end{pmatrix}, \quad (2)$$

in the  $(i, j)$  subblock, with

$$c_{ij} \equiv \cos \theta_{ij} \quad s_{ij} \equiv \sin \theta_{ij} \quad \tilde{s}_{ij} \equiv s_{ij} e^{-i\delta_{ij}}. \quad (3)$$

The parameterization in Eq. (1) has the following properties: (i) For vanishing mixing involving the fourth state ( $\theta_{14} = \theta_{24} = \theta_{34} = 0$ ) it reduces to the 3-flavor mixing matrix in its standard parameterization [26] with the identification  $\delta_{13} \equiv \delta$ . (ii) The leftmost positioning of the matrix  $\tilde{R}_{34}$  allows us to eliminate the mixing angle

$\theta_{34}$  (and the related  $CP$  phase  $\delta_{34}$ ) from the expression of the  $\nu_\mu \rightarrow \nu_e$  conversion probability in vacuum. In matter, the transition probability depends also on  $\theta_{34}$  and  $\delta_{34}$ . However, the sterile-induced matter perturbations are extremely small in T2K and such dependency is completely negligible (see the Appendix). (iii) For small values of  $\theta_{13}$  and of the mixing angles involving the fourth mass eigenstate, one has  $|U_{e3}|^2 \simeq s_{13}^2$ ,  $|U_{e4}|^2 = s_{14}^2$  (exact),  $|U_{\mu 4}|^2 \simeq s_{24}^2$  and  $|U_{\tau 4}|^2 \simeq s_{34}^2$ , with a clear physical interpretation of the new mixing angles.

Before considering the 4-flavor transition probability relevant for T2K, we recall a basic property of the 3-neutrino framework, which will be helpful in understanding the more general 4-neutrino case. In the presence of CPV, at LBL experiments one expects a nonzero value of the asymmetry

$$A_{\mu e}^{\text{CP}} \equiv P(\nu_\mu \rightarrow \nu_e) - P(\bar{\nu}_\mu \rightarrow \bar{\nu}_e), \quad (4)$$

which, in the 3-flavor (vacuum) case can be expressed as

$$A_{\mu e}^{\text{CP}} = 16 J \sin \Delta_{12} \sin \Delta_{23} \sin \Delta_{31}, \quad (5)$$

where  $\Delta_{ij} \equiv \Delta m_{ij}^2 L/4E$  ( $L$  being the baseline and  $E$  the neutrino energy) and  $J$  is the Jarlskog invariant [27]

$$J = \text{Im}[U_{e2} U_{\mu 3} U_{e3}^* U_{\mu 2}^*]. \quad (6)$$

The mass pattern chosen by nature for the three mass eigenstates is such that in the LBL setups we have  $\Delta \equiv \Delta_{13} \simeq \Delta_{23} \sim O(1)$  and  $\Delta_{12} = \alpha \Delta$ , with<sup>3</sup>  $|\alpha| \simeq 0.03$ . Consider, however, an ideal case where in the same setups we have  $|\Delta| \equiv |\Delta_{13}| \simeq |\Delta_{23}| \gg 1$ , while leaving  $\Delta_{12}$  unaltered (this would correspond to a much larger value of  $|\Delta m_{13}^2|$ ). In this situation, the average over the finite energy resolution of the experiment would wash out the fast oscillating terms in Eq. (5), giving rise to

$$-\langle \sin \Delta_{23} \sin \Delta_{31} \rangle \simeq \langle \sin^2 \Delta \rangle = 1/2, \quad (7)$$

thus obtaining for the  $CP$  asymmetry

$$\langle A_{\mu e}^{\text{CP}} \rangle = -8 J \sin \Delta_{12}. \quad (8)$$

This ideal case shows that CPV is not erased by the average over the two large frequencies. CPV cancellation would occur only if the third frequency were also very large ( $\Delta_{12} \gg 1$ ). Consider now a realistic 3+1 scheme. In this case, the oscillations induced by the three new large oscillation frequencies  $|\Delta_{new}| \equiv |\Delta_{14}| \simeq |\Delta_{24}| \simeq |\Delta_{34}| \gg 1$  will get averaged, and the information on their values will be lost. On the other hand, CPV effects will survive, since there are other two finite frequencies, the atmospheric [ $|\Delta| \equiv |\Delta_{13}| \simeq |\Delta_{23}| \sim O(1)$ ] and the solar

<sup>2</sup> An equally convenient choice is obtained by associating one of the new  $CP$  phases to  $R_{24}$  instead of  $R_{14}$ , i.e. by replacing the product  $R_{24} \tilde{R}_{14}$  with  $\tilde{R}_{24} R_{14}$ .

<sup>3</sup> Note that the sign of both  $\Delta \equiv \Delta_{13}$  and  $\alpha \equiv \Delta_{12}/\Delta_{13}$  changes with a swap of the mass hierarchy ( $\Delta_{13} \rightarrow -\Delta_{13}$ ), while the sign of the product  $\alpha \Delta$  is invariant (positive).

one ( $\Delta_{12} = \alpha\Delta$ ). Therefore, it will be natural to expect a dependency on the  $CP$ -phases in the flavor conversion process.

Let us now come to the expression of the  $\nu_\mu \rightarrow \nu_e$  transition probability probed in T2K. We recall that in the 3-flavor vacuum case, such a probability can be written as the sum of three terms

$$P_{\mu e}^{3\nu} = P^{\text{ATM}} + P^{\text{SOL}} + P^{\text{INT}}, \quad (9)$$

where the first two terms are positive definite probabilities induced by the atmospheric and the solar squared-mass splittings, while the third is generated by their interference and can assume both positive and negative values. An expansion in the small parameters  $s_{13} \simeq 0.15$  and  $\alpha \simeq \pm 0.03$  (supposed to have the same order  $\epsilon$ ) provides, at the second order in  $\epsilon$ , the well-known expressions [28]

$$P_{3\nu}^{\text{ATM}} \simeq 4s_{23}^2 s_{13}^2 \sin^2 \Delta, \quad (10)$$

$$P_{3\nu}^{\text{SOL}} \simeq 4c_{12}^2 c_{23}^2 s_{12}^2 (\alpha\Delta)^2, \quad (11)$$

$$P_{3\nu}^{\text{INT}} \simeq 8s_{13}s_{12}c_{12}s_{23}c_{23}(\alpha\Delta) \sin \Delta \cos(\Delta + \delta_{13}). \quad (12)$$

While all these three terms are formally of the same (second) order in  $\epsilon$ , they have quite different sizes, since  $|\alpha|$  is much smaller than  $s_{13}$ . Around the first oscillation maximum ( $\Delta \sim \pi/2$ ) probed by T2K, the atmospheric term is  $\sim 5 \times 10^{-2}$ , the interference term is  $\sim 1.3 \times 10^{-2}$ , and the solar term is  $\sim 1.5 \times 10^{-3}$ . Indeed, a different kind of expansion, considering  $s_{13} \sim \epsilon$  and  $\alpha \sim \epsilon^2$ , is more appropriate, as already evidenced in [29]. In this case, an expansion at the third order gives only the (leading) atmospheric term ( $\sim \epsilon^2$ ) and the (subleading) interference term ( $\sim \epsilon^3$ ). At the fourth order one recovers the solar term  $\propto (\alpha\Delta)^2$  of Eq. (11), and two additional terms [29]. The first term can be interpreted as a tiny modification of the atmospheric term  $\delta P^{\text{ATM}} \propto s_{13}^4$ , and the second one as a very small change of the interference term  $\delta P^{\text{INT}} \propto s_{13}^3(\alpha\Delta)$ . All three fourth-order terms, for the T2K baseline, have size  $\lesssim 2 \times 10^{-3}$  and have negligible impact.

Let us now come to the 4-flavor case. The analyses of the SBL anomalies [13, 14] point towards values of  $s_{14}$  and  $s_{24}$  which have sizes very similar to  $s_{13}$ . Hence, for the purposes of this work, which is limited to the SBL-preferred region, it is meaningful to assume that all these parameters have the same common order  $\epsilon$  and to consider  $\alpha \sim \epsilon^2$ . After averaging over the fast oscillations induced by the large frequency  $\Delta_{14}$ , at the fourth order in  $\epsilon$ , we find

$$\begin{aligned} P_{\mu e}^{4\nu} &\simeq (1 - s_{14}^2 - s_{24}^2)P_{\mu e}^{3\nu} \\ &+ 4s_{14}s_{24}s_{13}s_{23} \sin \Delta \sin(\Delta + \delta_{13} - \delta_{14}) \\ &- 4s_{14}s_{24}c_{23}s_{12}c_{12}(\alpha\Delta) \sin \delta_{14} \\ &+ 2s_{14}^2 s_{24}^2. \end{aligned} \quad (13)$$

The first term is the 3-flavor probability multiplied by the suppression factor  $f = 1 - O(\epsilon^2)$ . The second and third

terms can be ascribed, respectively, to the interference of the atmospheric and solar frequencies with the new large frequency, which does not appear in the formulas since it has been averaged out. The last term can be interpreted as the averaged transition probability in an effective 2-flavor description. As might have been expected, the transition probability is the sum of six contributions

$$\begin{aligned} P_{\mu e}^{4\nu} &= P^{\text{ATM}} + P^{\text{SOL}} + P^{\text{STR}} \\ &+ P_{\text{I}}^{\text{INT}} + P_{\text{II}}^{\text{INT}} + P_{\text{III}}^{\text{INT}}. \end{aligned} \quad (14)$$

The first two terms and the fourth one coincide (apart from the suppression factor  $f$ ) with the three standard 3-flavor terms in Eqs. (10)-(12). With  $P^{\text{STR}}$  we have indicated the last term in (13). The last two contributions are the new interference terms [the second and third terms in Eq. (13)]. Inspection of Eq. (13) reveals that  $P_{\text{II}}^{\text{INT}}$  is  $O(\epsilon^3)$  so its size is expected to be comparable to that of the standard inference term  $P_{\text{I}}^{\text{INT}}$  [see Eq. (12)]. Both  $P^{\text{STR}}$  and  $P_{\text{III}}^{\text{INT}}$  are  $O(\epsilon^4)$  like  $P^{\text{SOL}}$ .

Let us come back for a moment to Eq. (13). From this expression we can observe that the last three terms depend on the product  $s_{14}s_{24}$ , and, therefore, they depend on the effective appearance mixing angle, defined as

$$\sin 2\theta_{\mu e} \equiv 2|U_{e4}||U_{\mu 4}| \simeq 2s_{14}s_{24}, \quad (15)$$

which is the amplitude probed by the SBL  $\nu_\mu \rightarrow \nu_e$  appearance experiments. The first term in Eq. (13) depends on a different combination of the two mixing angles. However, in the particular case  $s_{14}^2 = s_{24}^2$ , this combination can be expressed as

$$s_{14}^2 + s_{24}^2 = 2s_{14}^2 = 2s_{14}s_{24} = \sin 2\theta_{\mu e}, \quad (16)$$

and the suppression factor  $f$  as<sup>4</sup>

$$f = 1 - \sin 2\theta_{\mu e}. \quad (17)$$

Therefore, in this particular case, Eq. (13) can be recast in the form

$$\begin{aligned} P_{\mu e}^{4\nu} &= (1 - \sin 2\theta_{\mu e})P_{\mu e}^{3\nu} \\ &+ 2 \sin 2\theta_{\mu e} s_{13}s_{23} \sin \Delta \sin(\Delta + \delta_{13} - \delta_{14}) \\ &- 2 \sin 2\theta_{\mu e} c_{23}s_{12}c_{12}(\alpha\Delta) \sin \delta_{14} \\ &+ \frac{1}{2} \sin^2 2\theta_{\mu e}, \end{aligned} \quad (18)$$

in which all the terms [and consequently all six terms in Eq. (14)] scale with a definite power of the effective appearance mixing angle.

As a result, in the particular case  $s_{14}^2 = s_{24}^2$ , the comparison of the terms involved in the transition probability is straightforward. Figure 1 displays (for  $\Delta = \pi/2$

<sup>4</sup> It is useful to observe that for a fixed value of the appearance angle  $\sin 2\theta_{\mu e}$ , the suppression factor  $f$  is always smaller than the one obtained in the specific case  $s_{14}^2 = s_{24}^2$ . In fact, the inequality  $(s_{14} - s_{24})^2 \geq 0$  implies that  $s_{14}^2 + s_{24}^2 \geq 2s_{14}s_{24} = \sin 2\theta_{\mu e}$ .

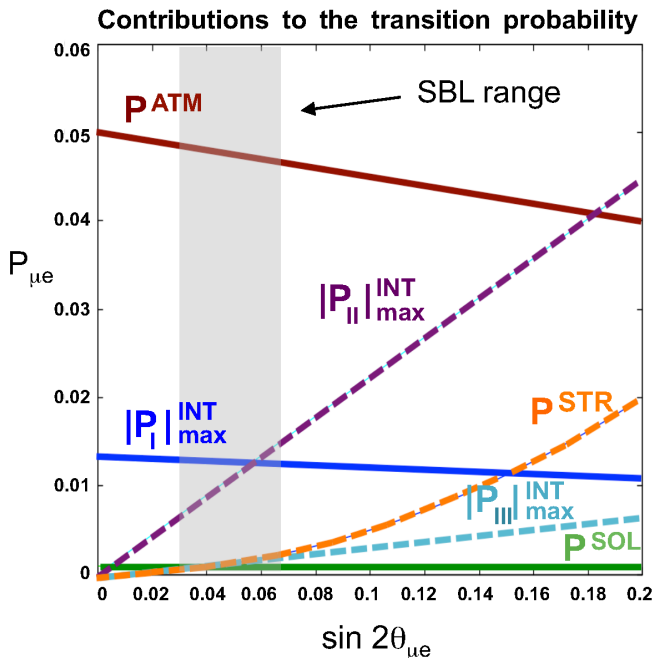


FIG. 1: Behavior of the six contributions to the transition probability in Eq. (14) as a function of the effective appearance mixing angle  $\sin 2\theta_{\mu e}$  in the case  $s_{14}^2 = s_{24}^2$  for  $s_{13}^2 = 0.025$ . The maximum absolute value is plotted for the three interference terms. The curves correspond to the first oscillation maximum  $\Delta = \pi/2$  (obtained for  $E_\nu \simeq 0.6$  GeV in T2K).

and  $s_{13}^2 = 0.025$ ) the behavior of all the six contributions in Eq. (14) as a function of  $\sin 2\theta_{\mu e}$ . We plot the maximum absolute value for the three interference terms (which can be positive or negative). The vertical gray band indicates the range allowed by the SBL anomalies. As expected from the discussion above, in this range, only the leading atmospheric and the two subleading interference terms are relevant, and the 4-flavor transition probability is approximately given by

$$P_{\mu e}^{A\nu} \simeq P^{\text{ATM}} + P_I^{\text{INT}} + P_{II}^{\text{INT}}. \quad (19)$$

Remarkably, the amplitude of the new (atmospheric-sterile) interference term is almost identical to that of the standard (solar-atmospheric) interference term. As a consequence, a big impact is expected on the regions reconstructed by the experiment T2K for the  $CP$ -phase  $\delta_{13}$ . More importantly, a similar sensitivity to the two  $CP$ -phases  $\delta_{13}$  and  $\delta_{14}$  is expected in the combination of T2K with the reactor experiments. The quantitative verification of these qualitative expectations will be the subject of the next section.

### III. NUMERICAL ANALYSIS

In our numerical analysis we include the reactor experiments Daya Bay and RENO and the LBL experiment

T2K. Concerning T2K the analysis is slightly different for the two cases of 3 and 4 flavors, since in this last case there are appreciable oscillation effects not only at the far detector (FD), Super-Kamiokande, but also at the near detector (ND), ND280, which must be taken into account. For this reason, we discuss the two cases separately. In the calculation of the oscillation probability we have included the MSW effects following the prescriptions described in the Appendix.

#### A. Treatment of the reactor experiments

The analysis of the reactor experiments is performed using the total rate information and following the approach described in detail in [30]. For both experiments we have used the latest data presented at the Neutrino 2014 Conference [4, 7] based on 621 live days (Daya Bay) and 800 live days (RENO). Since the electron antineutrino survival probability probed by these experiments is independent of the  $CP$ -violating phases (standard and nonstandard), their estimate of  $\theta_{13}$  does not depend on their values. We recall that such an estimate is extracted using the ratio of the event rates measured at the far and the near sites. Since the fast oscillations induced by  $\Delta m_{14}^2$  are averaged out at both detector sites, Daya Bay and RENO are not sensitive to 4-flavor effects. As a result, their estimate of  $\theta_{13}$  is independent of the mixing angle  $\theta_{14}$  provided that it is confined to vary in the range we are exploring.<sup>5</sup> Finally, it must be noted that the estimate of  $\theta_{13}$  is essentially identical for the two cases of normal hierarchy (NH) and inverted hierarchy (IH).

#### B. Treatment of T2K

##### 1. The 3-flavor case

We use the T2K results of the  $\nu_\mu \rightarrow \nu_e$  appearance searches [2], which reported 28 events with an estimated background of 4.92 events. In order to calculate the theoretical expectation for the total number of events and their binned spectrum in the reconstructed neutrino energy, we convolve the product of the  $\nu_\mu$  flux [31] (tables provided on the T2K home page [32]), the charged current quasielastic cross-section (estimated from [2]), and the  $\nu_\mu \rightarrow \nu_e$  transition probability, with an appropriate energy resolution function, which incorporates the correlation among the true and the reconstructed neutrino energy. For the energy resolution we have adopted a Gaussian function with width  $\sigma_E = 15\% \sqrt{E}$ . We have checked that our prediction for the binned spectrum of

<sup>5</sup> It can be shown that corrections to this approximation arise at the order  $\epsilon^6$ , being proportional to  $s_{13}^2 s_{14}^4$ , and are completely negligible.



events is in very good agreement with that shown by the collaboration in [2]. We have performed the analysis using both the total rate information and the full spectrum, observing very small differences between the two cases. This is due to the limited statistics currently available, and to the effect of the smearing induced by the energy resolution. As explained in the next subsection, in the 4-flavor case we could consistently perform only a total rate analysis. Therefore, for homogeneity, in the 3-flavor case, we report the results obtained with the total rate information.

## 2. The 4-flavor case

In the case of 4-flavor oscillations the T2K near detector is sensitive to the oscillations induced by the new  $\Delta m_{14}^2$ , since at the baseline  $L^{\text{ND}} = 280$  m,  $\Delta_{14}^{\text{ND}} \sim O(1)$ . Regard this, it should be noted that the published neutrino fluxes  $\phi_\nu(E)$  (both those relative to ND280 and their extrapolations at Super-Kamiokande) are constrained with the measurements performed at the ND (see [31]). More precisely, the available fluxes are not the original output of the dedicated simulation programs, but are a “postfit” version of these. Basically, the fluxes are anchored to the ND measurements, compatibly with the pulls of the nuisance parameters of the model of the original (“prefit”) fluxes. The anchoring of the fluxes to the ND measurements introduces an overall normalization factor and appreciable energy distortions, the typical size of which is  $\sim 10\%$ . These effects can be appreciated, for example, in Fig. 1 of [2].

This procedure is designed for the 3-flavor case, in which the oscillation effects at the ND are negligible; the procedure in this case improves the estimate of the nonoscillated fluxes. In contrast, in the presence of 4-flavor effects, the available postfit fluxes are no more an accurate estimate of the nonoscillated fluxes, since they partially incorporate the effects of the 4-flavor oscillations occurred at the ND. In the range of the small mixing angles we are exploring in this work, at the ND it is expected an energy dependent suppression of the nonoscillated fluxes whose amplitude ( $\simeq 4s_{24}^2 = 0.1$ ) is modulated by the  $O(1)$  phase  $\Delta_{14}^{\text{ND}} = \Delta m_{14}^2 L^{\text{ND}}/4E$ . A suppression of this size is certainly allowed by the nuisance parameters of the flux model.<sup>6</sup> Therefore, for the range of parameters under considerations, the postfit fluxes completely incorporate the 4-flavor effects (if these are present). In this situation, it is problematic to perform an accurate 4-flavor spectral analysis from outside the T2K Collaboration, since one would need to model

the original fluxes (with their uncertainties) and perform a simultaneous fit of both the ND and the FD event spectra varying the oscillation parameters  $\theta_{24}$  and  $\Delta m_{14}^2$ . For these reasons we limit our work to a total rate analysis.

We have checked that in the range of  $\Delta m_{14}^2 \in [0.1 - 10]$  eV<sup>2</sup>, the total rate suppression at the ND varies in the range [2, 8]%. For definiteness, in the analysis we assume  $\Delta m_{14}^2 = 1$  eV<sup>2</sup>, for which the total rate suppression is  $\sim 4\%$ . Consequently, we have increased the normalization of the published  $\nu_\mu$  flux by the same amount. Since the FD total rate is proportional to the product of the nonoscillated flux and the transition probability  $P_{\mu e}$ , in the fit, a larger flux will be compensated by a lower  $P_{\mu e}$ . By observing that the leading term of  $P_{\mu e}$  is proportional to  $\sin^2 \theta_{13}$ , we can deduce that the estimate of  $\sin^2 \theta_{13}$  will be slightly smaller ( $\sim -3\%$ ) with respect to the 3-flavor case, as we have explicitly checked numerically. Therefore, when interpreting the results of the 4-flavor analysis, one should bear in mind that this (small) effect is at play, together with those (larger) described in Sec. II, which are genuine LBL effects.

We remark that the fake energy distortions introduced in the fluxes by the ND280 anchoring procedure are also present, basically unaltered, in the far detector fluxes (which are an extrapolation of the ND fluxes). For this reason, it would be pointless (and wrong) to perform a spectral 4-flavor analysis of the FD data using the published fluxes. As we have shown in the previous subsection on the 3-flavor analysis, the T2K sensitivity is currently dominated by the total rate information. Therefore, it is legitimate to expect that the total rate information will give accurate results in the 4-flavor case as well, provided that the fake distortions are of the order of a few per cent. Of course, the situation would be different for values of  $s_{24}^2$  much larger than those considered in this work, in which case a dedicated spectral analysis would be inescapable. The same conclusion would hold if the T2K  $\nu_\mu \rightarrow \nu_e$  appearance measurement had considerably larger statistics.

A final remark is in order concerning the treatment of the atmospheric mixing angle  $\theta_{23}$ . It can be shown that the far/near ratio in the  $\nu_\mu \rightarrow \nu_\mu$  channel is almost unaffected by 4-flavor effects, as we have explicitly checked numerically. Therefore, the estimate of  $\theta_{23}$  is expected to be very stable with respect to the 4-flavor perturbations induced by the small values of  $s_{24}^2$  we are considering. Therefore, in the 4-flavor analysis we have marginalized  $\theta_{23}$  taking into account the constraint  $\sin^2 \theta_{23} \simeq 0.51 \pm 0.055$  obtained, within the 3-flavor framework, from the  $\nu_\mu \rightarrow \nu_\mu$  disappearance measurement [33] performed by T2K. This assumption would not be justified for larger values of  $\theta_{24}$ , in which case the estimate of  $\theta_{23}$  should be obtained by analyzing the  $\nu_\mu \rightarrow \nu_\mu$  disappearance results within a 4-flavor framework.

<sup>6</sup> Indeed, the ND spectrum normalization appears to be a few per cent lower than the prefit one, most of the suppression being concentrated in a region close to the peak of the muon momentum distribution (see Fig. 1 of [2]).

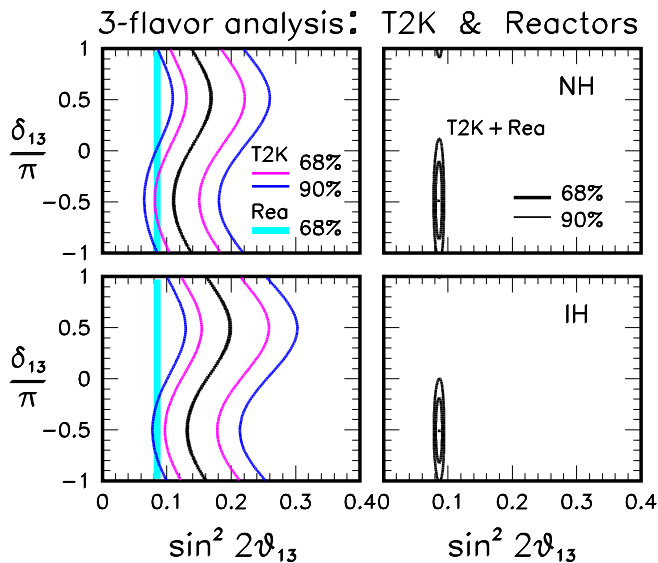


FIG. 2: Left panels: Regions allowed by T2K and by reactor experiments for normal hierarchy (upper panel) and inverted hierarchy (lower panel). Right panels: Regions allowed by their combination. The mixing angle  $\theta_{23}$  is marginalized away. The confidence levels refer to 1 d.o.f. ( $\Delta\chi^2 = 1.0, 2.71$ ).

### C. Results of the 3-flavor analysis

In the 3-flavor analysis, the two mixing angles ( $\theta_{13}$ ,  $\theta_{23}$ ) and the  $CP$ -phase  $\delta_{13}$  are treated as free parameters, taking into account the external prior  $\sin^2\theta_{23} \simeq 0.51 \pm 0.055$  provided by the  $\nu_\mu \rightarrow \nu_\mu$  disappearance mea-

surement [33] performed by T2K. For the atmospheric mass splitting we use the best-fit value of  $\Delta m_{13}^2$  obtained in the same analysis. The solar mass-mixing parameters are fixed at the best-fit value obtained in the global analysis [9].

Figure 2 shows the results of the analysis for the two cases of NH (upper panels) and IH (lower panels) in the plane spanned by the two variables  $[\sin^2 2\theta_{13}, \delta_{13}]$ , the atmospheric mixing angle  $\theta_{23}$  having been marginalized away. The left panels report the T2K-allowed regions for the confidence levels 68% and 90% (1 d.o.f), identical to those used by the T2K Collaboration, so as to facilitate comparison. Our results are basically superimposable to those obtained by the collaboration (see Fig. 5 in [2]). The thin vertical band displayed in both panels represents the range allowed at 68% C.L. for  $\theta_{13}$  by the reactor experiments. As already noticed in the global analyses [9–11] and in partial fits performed by various experimental collaborations, the T2K-allowed bands lie at values of  $\theta_{13}$ , which are somewhat larger compared to the range identified by reactors. As a result, as evident in the two right panels, the combination of the reactor experiments with T2K tends to select values of  $\delta \sim -\pi/2$ , disfavoring the cases of no CPV ( $\delta_{13} = 0, \pi$ ) at roughly the 90% C.L. In addition, a weak preference for the case of normal hierarchy emerges ( $\chi_{\text{NH}}^2 - \chi_{\text{IH}}^2 \simeq -0.8$ ).

### D. Results of the 4-flavor analysis

As discussed in detail in the Appendix, in the 3+1 scheme, the role of matter effects is very similar to the

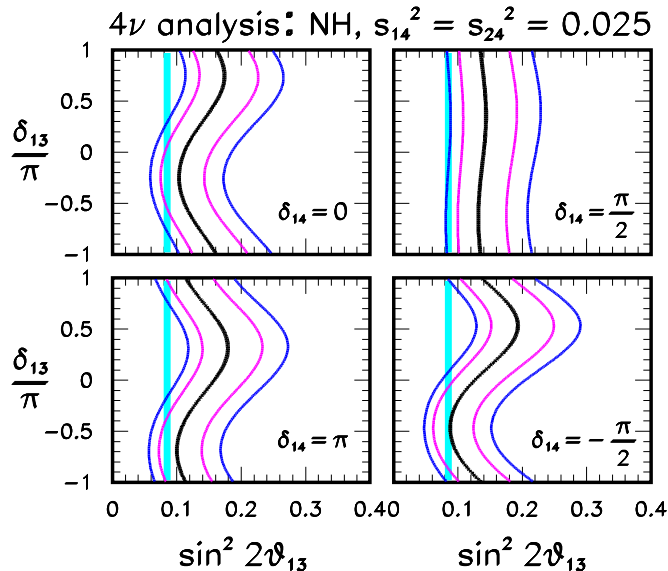


FIG. 3: Regions allowed by T2K for four values of the  $CP$ -phase  $\delta_{14}$ . Normal hierarchy is assumed. The mixing angle  $\theta_{23}$  is marginalized away. The vertical band represents the region allowed by reactor experiments. Confidence levels are as in Fig. 2.

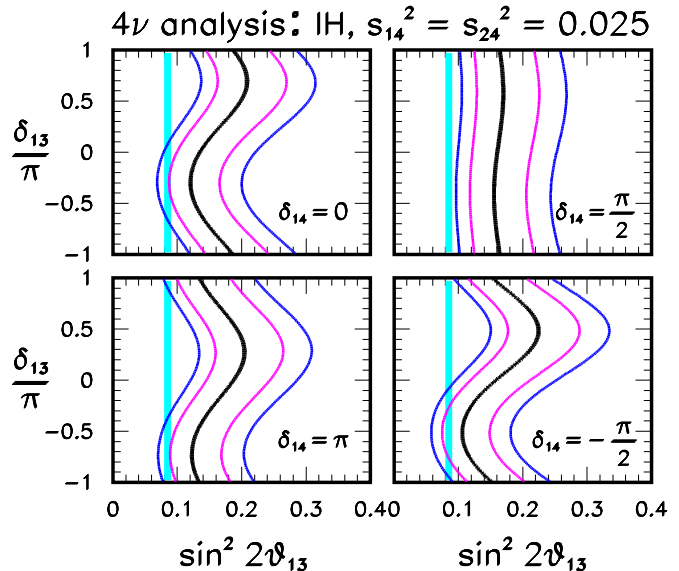


FIG. 4: Regions allowed by T2K for four values of the  $CP$ -phase  $\delta_{14}$ . Inverted hierarchy is assumed. The vertical band represents the region allowed by reactor experiments. The mixing angle  $\theta_{23}$  is marginalized away. Confidence levels are as in Fig. 2.

3-flavor case. Basically (in comparison to the vacuum case), they tend to increase (decrease) the theoretically expected T2K rate in the case of NH (IH), with a consequent downward (upward) shift of the range preferred for  $\theta_{13}$ . The “wiggle” structure of the allowed regions is basically the same for the two mass hierarchies (see Figs. 3 and 4). The regions obtained for the case of IH are essentially shifted towards larger values of  $\theta_{13}$  and slightly expanded with respect to those obtained in the NH case. We describe in detail the results only for NH, the interpretation of the IH case being straightforward.

Figure 3 displays the results of the 4-flavor analysis for the case of NH. The four panels represent the T2K-allowed regions in the usual plane  $[\sin^2 2\theta_{13}, \delta_{13}]$  for four different choices of the new  $CP$ -phase  $\delta_{14}$ . We have fixed the 4-flavor parameters at the following values:  $s_{14}^2 = s_{24}^2 = 0.025$ ,  $s_{34}^2 = 0$ ,  $\delta_{34} = 0$  and  $\Delta m_{14}^2 = 1 \text{ eV}^2$ . As a benchmark we also report the range allowed for  $\theta_{13}$  by reactors, which is identical to the standard case. A quick comparison of the four panels of Fig. 3 with the 3-flavor case (left upper panel of Fig. 2) shows the large impact of the 4-flavor effects on the structure of the T2K wiggles. The behavior of the curves can be easily interpreted, taking into account that the dominant contribution to the total rate comes from a region of the energies close to the first oscillation maximum, where  $\Delta \sim \pi/2$ . Inspection of Eq. (12) shows that the standard interference term is proportional to  $-\sin \delta_{13}$ . From Eq. (13) we see that for  $\delta_{14} = \pi/2$ , the new interference term is proportional to  $\sin \delta_{13}$ . Therefore, in this case the two terms are in opposition of phase and having similar amplitudes their sum tends to cancel out, making the wiggles almost

disappear (right upper panel). In this case, the T2K region is basically a vertical band.

For  $\delta_{14} = -\pi/2$  (right lower panel of Fig. 3) the two inference terms have the same phase and the horizontal excursion of the wiggles is increased (roughly doubled). As a benchmark, the best-fit curve excursion range is  $[0.11, 0.17]$  in the 3-flavor case, while it is  $[0.09, 0.19]$  in the 4-flavor one. In the two cases  $\delta_{14} = 0, \pi$  (left panels of Fig. 3) the new interference term is proportional to  $\pm \cos \delta_{13} = \pm \sin(\pi/2 - \delta_{13})$  and, thus, it has a  $\pm \pi/2$  difference of phase with respect to the standard one. As a result, in those two cases, the behavior of the T2K bands is intermediate between the two cases  $\delta_{14} = (-\pi/2, \pi/2)$ .

It is interesting to note that, in the presence of 4-flavor effects, a better agreement between the estimates of  $\theta_{13}$  from reactors and T2K can be obtained. In particular, this occurs for  $\delta_{14} \simeq -\pi/2$ , which is, therefore, expected to be the best-fit value in the combined analysis of reactors with T2K. We recall that a (small) part of the shift towards lower values of  $\theta_{13}$  of the T2K bands is imputable to the re-normalization of the nonoscillated  $\nu_\mu$  flux, which we have incorporated in our analysis in order to take into account the effect of the oscillations at the near detector ND280 (see the discussion in subsection III.A.2).

As a last step in our 4-flavor analysis, we perform the combination of T2K with reactors. In this more general analysis, we treat the two mixing angles ( $\theta_{13}, \theta_{23}$ ) and the two  $CP$ -phases ( $\delta_{13}, \delta_{14}$ ) as free parameters, while fixing the remaining 4-flavor parameters at the same values used before:  $s_{14}^2 = s_{24}^2 = 0.025$ ,  $s_{34}^2 = 0$ ,  $\delta_{34} = 0$

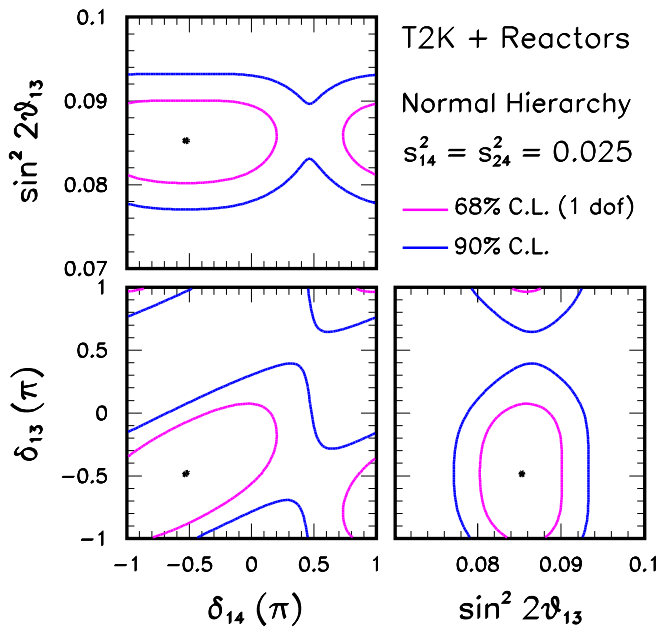


FIG. 5: Regions allowed by the combination of T2K and reactor experiments for the case of normal hierarchy. The mixing angle  $\theta_{23}$  is marginalized away.

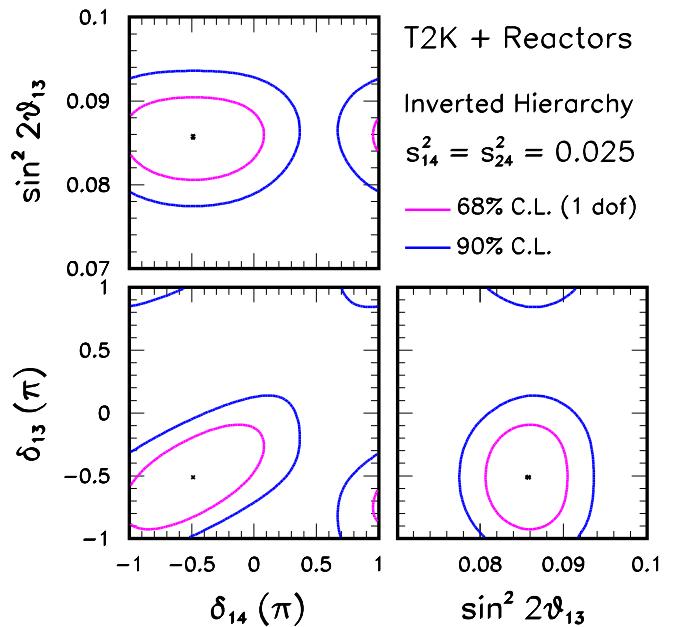


FIG. 6: Regions allowed by the combination of T2K and reactor experiments for the case of inverted hierarchy. The mixing angle  $\theta_{23}$  is marginalized away.

and  $\Delta m_{14}^2 = 1 \text{ eV}^2$ . We have checked that the impact of nonzero  $\theta_{34}$  (and consequently of the associated  $CP$ -phase  $\delta_{34}$ ) is negligible, even considering very large values of  $\theta_{34}$ , well beyond the current bounds. Therefore, the results of the analysis, albeit formally obtained for the fixed value  $\theta_{34} = 0$ , are indeed more general and are equivalent to those that one would obtain by treating  $\theta_{34}$  and  $\delta_{34}$  as free parameters and marginalizing over them. The insensitivity to  $\theta_{34}$  in vacuum is obvious from the formulas presented in Sec. II. The reason of its irrelevance also in matter is explained in the Appendix.

Similar to the 3-flavor case, in the T2K + reactors combination, the ( $CP$ -phases-independent) estimate of  $\theta_{13}$  provided by the reactor experiments selects those subregions of the T2K bands that have a statistically significant overlap with such an estimate. These, in turn, correspond to allowed regions in the plane  $[\delta_{13}, \delta_{14}]$  spanned by the two  $CP$ -phases. Figures 5 and 6 display such regions for the two cases of NH and IH, together with the 2-dimensional projections that have the mixing angle  $\theta_{13}$  as one of the two variables. As expected a preference for values of  $\delta_{13} \sim \delta_{14} \sim -\pi/2$  emerges. The absence of  $CP$  violation is disfavored at a slightly lower confidence level in comparison with the 3-flavor case. This is imputable to the larger freedom allowed by the larger parameter space available in the 3+1 scheme.

#### IV. CONCLUSIONS AND OUTLOOK

We have investigated the impact of light ( $\sim \text{eV}$ ) sterile neutrinos in the long-baseline experiment T2K. We have shown that, within the 3+1 scheme, for mass-mixing parameters suggested by the short-baseline anomalies, the new term appearing in the  $\nu_\mu \rightarrow \nu_e$  transition probability arising from the interference between the sterile and the atmospheric oscillation frequencies has the same order of magnitude of the standard 3-flavor solar-atmospheric interference term. As a result, the current T2K data (in combination with the  $\theta_{13}$ -dedicated reactor experiments) are sensitive to two of the three  $CP$ -violating phases involved in the 3+1 scheme. In particular, we found that both the standard phase and the new one ( $\delta_{13} \equiv \delta$  and  $\delta_{14}$  in our parameterization choice) tend to have a common best-fit value  $\delta_{13} \simeq \delta_{14} \sim -\pi/2$ . In addition, quite intriguingly, our analysis shows that the inclusion of sterile neutrino effects leads to better agreement of the two estimates of  $\theta_{13}$  obtained, respectively, from T2K and reactor data.

Our results make it evident that T2K and other similar LBL experiments (like MINOS and NO $\nu$ A in the near future) should be routinely included in the global fits involving sterile neutrinos. Finally, we stress that, in the eventuality of a discovery of light sterile neutrino species at the upcoming SBL experiments, our findings would represent the first indications on the sterile-induced CPV sources. The LBL accelerator experiments that are already operational, and those planned for the

future (LBNE, LBNO, and T2HK), will play a key role in extracting more information on the new CPV sector, the exploration of which has, with the present work, just begun.

#### APPENDIX: TREATMENT OF THE MSW EFFECT

The Hamiltonian in the flavor basis can be written as

$$H = UKU^\dagger + V, \quad (20)$$

where  $K$  denotes the diagonal matrix containing the wave numbers  $k_i = m_i^2/2E$  ( $i = 1, 2, 3, 4$ ) ( $m_i^2$  and  $E$  being the neutrino squared-mass and energy respectively), while the matrix  $V$  incorporates the position-independent matter MSW potential [34, 35]. Barring irrelevant factors proportional to the identity, we can define the diagonal matrix containing the three relevant wave numbers as

$$K = \text{diag}(0, k_{12}, k_{13}, k_{14}) \quad (21)$$

and the matrix encoding the matter effects, as

$$V = \text{diag}(V_{CC}, 0, 0, -V_{NC}), \quad (22)$$

where

$$V_{CC} = \sqrt{2}G_F N_e \quad (23)$$

is the charged-current interaction potential of the electron neutrinos with the background electrons having number density  $N_e$ , and

$$V_{NC} = -\frac{1}{2}\sqrt{2}G_F N_n \quad (24)$$

is the neutral-current interaction potential (common to all the active neutrino species) with the background neutrons having number density  $N_n$ . For later convenience, we also introduce the positive-definite ratio

$$r = -\frac{V_{NC}}{V_{CC}} = \frac{1}{2} \frac{N_n}{N_e}, \quad (25)$$

which in the Earth crust is approximately  $r \simeq 0.5$ . In order to simplify the treatment of matter effects in LBL experiments it is useful to introduce the new basis

$$\bar{\nu} = \bar{U}^\dagger \nu, \quad (26)$$

where

$$\bar{U} = \tilde{R}_{34} R_{24} \tilde{R}_{14} \quad (27)$$

is the part of the mixing matrix defined in Eq. (1) containing only the rotations involving the fourth neutrino mass state. In this new basis, the Hamiltonian assumes the form

$$\bar{H} = \bar{H}^{\text{kin}} + \bar{H}^{\text{dyn}} = U_{3\nu} K U_{3\nu}^\dagger + \bar{U}^\dagger V \bar{U}, \quad (28)$$



where the first term is the kinematic contribution describing the oscillations in vacuum, and the second one represents a nonstandard dynamical term. Since  $|k_{14}|$  is much bigger than  $k_{12}$  and  $|k_{13}|$  and much bigger than 1, we can reduce the dynamics to that of an effective 3-flavor system. Indeed, from Eq. (28) one has that the (4,4) entry of  $\bar{H}$  is much bigger than all the other elements and (the absolute value of) the fourth eigenvalue of  $\bar{H}$  is much larger than the other three ones. As a result, the state  $\bar{\nu}_s$  evolves independently of the others. Extracting from  $\bar{H}$  the submatrix with indices (1, 2, 3), one obtains the  $3 \times 3$  Hamiltonian

$$\bar{H}_{3\nu} = \bar{H}_{3\nu}^{\text{kin}} + \bar{H}_{3\nu}^{\text{dyn}} \quad (29)$$

governing the evolution of the  $(\bar{\nu}_e, \bar{\nu}_\mu, \bar{\nu}_\tau)$  system, whose dynamical part has the form

$$\bar{H}^{\text{dyn}} = V_{CC} \begin{pmatrix} |\bar{U}_{e1}|^2 + r|\bar{U}_{s1}|^2 & r\bar{U}_{s1}^* \bar{U}_{s2} & r\bar{U}_{s1}^* \bar{U}_{s3} \\ \dagger & r|\bar{U}_{s2}|^2 & r\bar{U}_{s2}^* \bar{U}_{s3} \\ \dagger & \dagger & r|\bar{U}_{s3}|^2 \end{pmatrix}, \quad (30)$$

where, for brevity, we have indicated with  $\dagger$  the complex conjugate of the matrix element having the same two indices inverted. In deriving Eq. (30) we have made use of the relations  $\bar{U}_{e2} = \bar{U}_{e3} = \bar{U}_{\mu 3} = 0$ . Considering the explicit expressions of the elements of  $\bar{U}$ , Eq. (30) takes the form

$$\bar{H}^{\text{dyn}} = V_{CC} \begin{pmatrix} c_{14}^2 + r c_{34}^2 c_{24}^2 s_{14}^2 & r c_{34}^2 c_{24} \bar{s}_{14} s_{24} & r c_{34} c_{24} \bar{s}_{14} \bar{s}_{34}^* \\ \dagger & r c_{34}^2 s_{24}^2 & r c_{34} s_{24} \bar{s}_{34}^* \\ \dagger & \dagger & r s_{34}^2 \end{pmatrix} \quad (31)$$

which, for vanishing sterile neutrino angles ( $\theta_{14} = \theta_{24} = \theta_{34} = 0$ ) returns the standard 3-flavor MSW potential. For small values of such mixing angles, the dynamical term is approximated by

$$\bar{H}^{\text{dyn}} \approx V_{CC} \begin{pmatrix} 1 - (1-r)s_{14}^2 & r\bar{s}_{14}s_{24} & r\bar{s}_{14}\bar{s}_{34}^* \\ \dagger & r s_{24}^2 & r s_{24} \bar{s}_{34}^* \\ \dagger & \dagger & r s_{34}^2 \end{pmatrix}. \quad (32)$$

This shows that the corrections to the standard potential are of second order<sup>7</sup> in the new  $s_{ij}$ 's and further suppressed by a factor  $r$  or  $(1-r)$ ; in the Earth crust,  $r \sim 0.5$ . Therefore, for realistic values of the mixing angles, these corrections are  $O(\epsilon^2)$ , and hence at the level of a few per cent. Taking into account that in T2K the *standard* matter effects are also small, being  $v = V_{CC}/|k_{13}| \sim 0.05$ , we can deduce that the new nonstandard effects have amplitudes of a few per mill and have a completely negligible impact. We have numerically checked that allowing for very large values of  $\theta_{34}$  (which is the least known of the three new mixing angles) even beyond the range currently allowed by the global fits, the transition probability is basically indistinguishable from the case of  $\theta_{34} = 0$ . Therefore, the independence of the transition probability from

$\theta_{34}$ , which is exact in vacuum, remains essentially valid also in the presence of matter effects.

For the calculation of the transition probability, it is useful to define the evolution operator, which, in the rotated basis, takes the form

$$\bar{S} \equiv e^{-i\bar{H}L} \approx \begin{pmatrix} e^{-i\bar{H}_{3\nu}L} & \mathbf{0} \\ \mathbf{0} & e^{-ik_{14}L} \end{pmatrix}, \quad (33)$$

and is connected to the evolution operator in the original flavor basis through the unitary transformation

$$S = \bar{U}\bar{S}\bar{U}^\dagger. \quad (34)$$

Taking into account the block-diagonal form of  $\bar{S}$  and the relations  $\bar{U}_{e2} = \bar{U}_{e3} = \bar{U}_{\mu 3} = 0$ , one has for the relevant transition amplitude

$$S_{e\mu} = \bar{U}_{e1} [\bar{U}_{\mu 1}^* \bar{S}_{ee} + \bar{U}_{\mu 2}^* \bar{S}_{e\mu}] + \bar{U}_{e4} \bar{U}_{\mu 4}^* \bar{S}_{ss}. \quad (35)$$

Since  $\bar{S}_{ss} = e^{-ik_{14}L}$  oscillates very fast, the associated terms are averaged out by the finite energy resolution of the detector, and for the transition probability we have

$$P_{\mu e}^{4\nu} \equiv |S_{e\mu}|^2 = |\bar{U}_{e1}|^2 |\bar{U}_{\mu 1}|^2 |\bar{S}_{ee}|^2 + |\bar{U}_{e1}|^2 |\bar{U}_{\mu 2}|^2 |\bar{S}_{e\mu}|^2 + 2|\bar{U}_{e1}|^2 \text{Re}[\bar{U}_{\mu 1}^* \bar{U}_{\mu 2} \bar{S}_{ee} \bar{S}_{e\mu}^*] + |\bar{U}_{e4}|^2 |\bar{U}_{\mu 4}|^2. \quad (36)$$

This expression is completely general, except for the assumption of averaged oscillations, and connects the 4-flavor transition probability to the amplitudes of the effective 3-flavor system governed by the effective Hamiltonian in Eq. (29). Considering the explicit expressions of the elements of the matrix  $\bar{U}$ , Eq. (36) becomes

$$P_{\mu e}^{4\nu} = c_{14}^2 s_{24}^2 s_{14}^2 \bar{P}_{ee}^{3\nu} + c_{14}^2 c_{24}^2 \bar{P}_{\mu e}^{3\nu} - 2c_{14}^2 c_{24} s_{14} s_{24} \text{Re}(e^{-i\delta_{14}} \bar{S}_{ee} \bar{S}_{e\mu}^*) + c_{14}^2 s_{14}^2 s_{24}^2, \quad (37)$$

where  $\bar{P}_{ee}^{3\nu} \equiv |\bar{S}_{ee}|^2$  and  $\bar{P}_{\mu e}^{3\nu} \equiv |\bar{S}_{e\mu}|^2$ . Therefore, the 4-flavor problem is reduced to a more familiar 3-flavor one, for which one needs to calculate the elements  $\bar{S}_{ee}$  and  $\bar{S}_{e\mu}$ .

Figure 7 shows the fast oscillating transition probability obtained by a full 4-flavor numerical evolution and the averaged probability calculated using Eq. (37) for the best-fit values  $\delta_{13} = \delta_{14} = -\pi/2$ . For clarity we have chosen the value  $\Delta m_{14}^2 = 0.1 \text{ eV}^2$ . Figure 8 displays some selected examples of the 4-flavor probability calculated using Eq. (37). The four panels correspond to four different values of the standard  $CP$ -phase  $\delta_{13}$ . In each panel, the black thick solid line represents the 3-flavor case ( $\theta_{14} = \theta_{24} = 0$ ), while the colored lines represent the 4-flavor case (with  $s_{14}^2 = s_{24}^2 = 0.025$ ) for four different values of the nonstandard  $CP$ -phase:  $\delta_{14} = 0$

<sup>7</sup> A similar behavior has been observed to occur in solar neutrino transitions induced by sterile species [36].

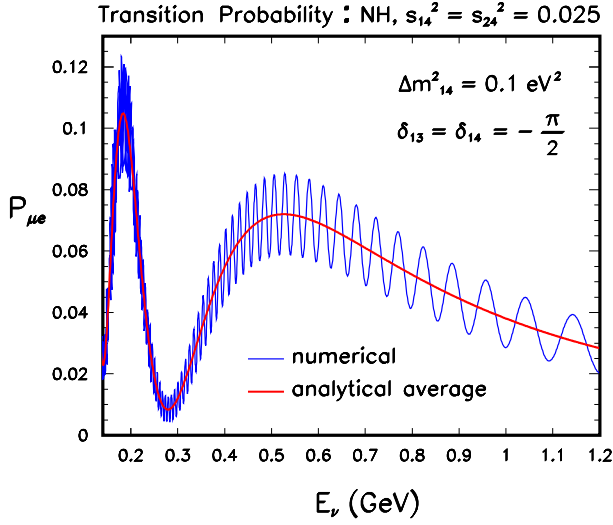


FIG. 7: Probability of  $\nu_\mu \rightarrow \nu_e$  transition in the 3+1 scheme. The thin blue line represents the numerical result, while the red line represents the averaged probability obtained using Eq. (37). In both cases the hierarchy is normal and the mixing angles are fixed at the values  $s_{14}^2 = s_{24}^2 = 0.025$ .

(solid),  $\delta_{14} = \pi$  (long-dashed),  $\delta_{14} = \pi/2$  (short-dashed), and  $\delta_{14} = -\pi/2$  (dotted).

While the 3-flavor elements  $\bar{S}_{ee}$  and  $\bar{S}_{e\mu}$  can be evaluated numerically (as we have done) approximate expressions already existing in the literature in various limits

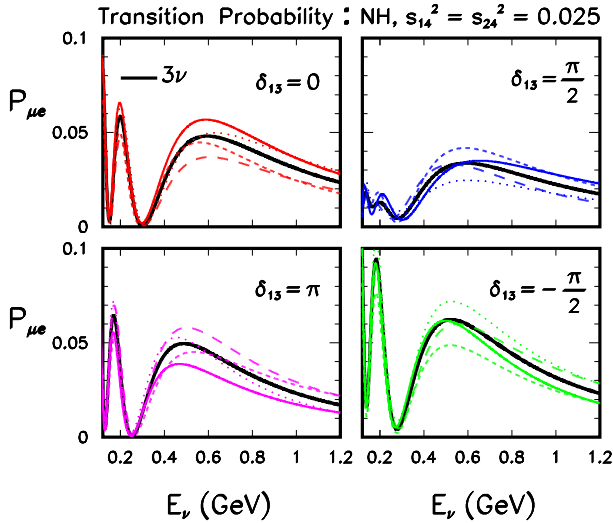


FIG. 8: Probability of  $\nu_\mu \rightarrow \nu_e$  transition in the 3+1 scheme for normal hierarchy. The four panels correspond to four different values of the standard  $CP$ -phase  $\delta_{13}$ . In each panel, the black thick solid line represents the 3-flavor case ( $\theta_{14} = \theta_{24} = 0$ ), while the colored lines represent the 4-flavor case (with  $s_{14}^2 = s_{24}^2 = 0.025$ ) for the following four different values of the nonstandard  $CP$ -phase:  $\delta_{14} = 0$  (solid),  $\delta_{14} = \pi$  (long-dashed),  $\delta_{14} = \pi/2$  (short-dashed), and  $\delta_{14} = -\pi/2$  (dotted).

may help to further simplify the expression of the transition probability in Eq. (37), which, for small values of the two mixing angles  $\theta_{14}$  and  $\theta_{24}$ , takes the form

$$P_{\mu e}^{4\nu} \simeq (1 - s_{14}^2 - s_{24}^2) \bar{P}_{\mu e}^{3\nu} - 2s_{14}s_{24} \text{Re}(e^{-i\delta_{14}} \bar{S}_{ee} \bar{S}_{e\mu}^*) + s_{14}^2 s_{24}^2 (1 + \bar{P}_{ee}^{3\nu}). \quad (38)$$

First, it can be noted that for small values of  $s_{13} \sim \epsilon$  and  $\alpha\Delta \sim \epsilon^2$  one has [37]

$$\bar{S}_{ee} \simeq 1 - O(\epsilon^2). \quad (39)$$

Since we are interested to terms up to  $O(\epsilon^4)$ , we can assume  $\bar{S}_{ee} = 1$ . Moreover, as discussed above, the nonstandard matter effects are completely negligible and only the small standard matter effects are relevant. In this approximation, the 3-flavor amplitude  $\bar{S}_{e\mu}$  has the well-known (see, for example, [37]) form

$$\bar{S}_{e\mu} \simeq A s_{13}^m \sin \Delta^m + B(\alpha\Delta), \quad (40)$$

where  $A$  and  $B$  are two complex coefficients with  $O(1)$  modulus, given by

$$A = -2i s_{23} e^{-i(\Delta + \delta_{13})}, \quad (41)$$

$$B = -2i c_{23} s_{12} c_{12}, \quad (42)$$

and  $(s_{13}^m, \Delta^m)$  are the approximated expressions of  $(s_{13}, \Delta)$  in matter

$$s_{13}^m \simeq (1 + v) s_{13}, \quad (43)$$

$$\Delta^m \simeq (1 - v) \Delta, \quad (44)$$

with  $v = V_{CC}/|k_{13}| \simeq 0.05$ . Making use of Eqs. (39)-(44) in the expression of the transition probability in Eq. (38), in the limit case  $v = 0$  we recover, in an alternative way, the fourth-order expansion of the vacuum formula in Eq. (13) presented in Sec. II. For  $v \neq 0$ , one sees that the structure of the transition probability remains the same as in vacuum, containing six terms of which three are of the interference type. The only impact of matter effects (at least for the T2K setup) is to break the degeneracy between NH and IH, exactly as it occurs in the 3-flavor case, because of the shifts  $s_{13} \rightarrow s_{13}^m$  and  $\Delta \rightarrow \Delta^m$  in Eqs. (43),(44).

## Acknowledgments

A. P. acknowledges support from the European Community through a Marie Curie IntraEuropean Fellowship, Grant No. PIEF-GA-2011-299582, ‘‘On the Trails of New Neutrino Properties.’’ We acknowledge partial support from the European Union FP7 ITN Invisibles (Marie Curie Actions, Grant No. PITN-GA-2011-289442).

- 
- [1] N. Cabibbo, Phys. Lett. **72B**, 333 (1978).
- [2] K. Abe *et al.* (T2K Collaboration), Phys. Rev. Lett. **112**, 061802 (2014).
- [3] P. Adamson *et al.* (MINOS Collaboration), Phys. Rev. Lett. **112**, 191801 (2014).
- [4] C. Zhang (Daya Bay Collaboration), in XXVI International Conference on Neutrino Physics and Astrophysics, Boston, USA 2014 (to be published).
- [5] F. P. An *et al.* (Daya Bay Collaboration), Phys. Rev. Lett. **112**, 061801 (2014).
- [6] Y. Abe *et al.* (Double Chooz Collaboration), J. High Energy Phys. 10 (2014) 086.
- [7] S.-H. Seo (RENO Collaboration), in XXVI International Conference on Neutrino Physics and Astrophysics, Boston, USA, 2014 (to be published).
- [8] Y. Suzuki (Super-Kamiokande Collaboration), in NIAPP Topical Workshop, Munich Institute for Astro- and Particle Physics, 2014.
- [9] F. Capozzi, G. L. Fogli, E. Lisi, A. Marrone, D. Montanino, and A. Palazzo, Phys. Rev. D **89** (2014) 093018.
- [10] M. C. Gonzalez-Garcia, M. Maltoni, and T. Schwetz, J. High Energy Phys. 11 (2014) 052.
- [11] D. V. Forero, M. Tortola, and J. W. F. Valle, Phys. Rev. D **90**, 093006 (2014).
- [12] A. Palazzo, Mod. Phys. Lett. A **28**, 1330004 (2013).
- [13] J. Kopp, P. A. N. Machado, M. Maltoni, and T. Schwetz, J. High Energy Phys. 05 (2013) 050.
- [14] C. Giunti, M. Laveder, Y. F. Li, and H. W. Long, Phys. Rev. D **88**, 073008 (2013).
- [15] A. Donini and D. Meloni, Eur. Phys. J. C **22**, 179 (2001).
- [16] A. Donini, M. Lusignoli, and D. Meloni, Nucl. Phys. **624B**, 405 (2002).
- [17] A. Donini, M. Maltoni, D. Meloni, P. Migliozzi, and F. Terranova, J. High Energy Phys. 12 (2007) 013.
- [18] A. Dighe and S. Ray, Phys. Rev. D **76**, 113001 (2007).
- [19] A. Donini, K. i. Fuki, J. Lopez-Pavon, D. Meloni, and O. Yasuda, J. High Energy Phys. 08 (2009) 041.
- [20] O. Yasuda, arXiv:1004.2388.
- [21] D. Meloni, J. Tang, and W. Winter, Phys. Rev. D **82**, 093008 (2010).
- [22] B. Bhattacharya, A. M. Thalapillil, and C. E. M. Wagner, Phys. Rev. D **85**, 073004 (2012).
- [23] A. Donini, P. Hernandez, J. Lopez-Pavon, M. Maltoni, and T. Schwetz, J. High Energy Phys. 07 (2012) 161.
- [24] D. Hollander and I. Mocioiu, Phys. Rev. D **91**, 013002 (2015).
- [25] J. Schechter and J. W. F. Valle, Phys. Rev. D **22**, 2227 (1980).
- [26] K. Nakamura *et al.* (Particle Data Group), J. Phys. G **37**, 075021 (2010).
- [27] C. Jarlskog, Phys. Rev. Lett. **55**, 1039 (1985).
- [28] A. Cervera, A. Donini, M. B. Gavela, J. J. Gomez Cadenas, P. Hernandez, O. Mena, and S. Rigolin, Nucl. Phys. **579B**, 17 (2000); *ibid.* **593B**, 731 (E) (2001).
- [29] K. Asano and H. Minakata, J. High Energy Phys. 06 (2011) 022.
- [30] A. Palazzo, J. High Energy Phys. 10 (2013) 172.
- [31] K. Abe *et al.* (T2K Collaboration), Phys. Rev. D **87**, 012001 (2013).
- [32] <http://t2k-experiment.org/results/neutrino-beam-flux-2013/>.
- [33] K. Abe *et al.* (T2K Collaboration), Phys. Rev. Lett. **112**, 181801 (2014).
- [34] L. Wolfenstein, Phys. Rev. D **17**, 2369 (1978).
- [35] S. P. Mikheev and A. Yu. Smirnov, Sov. J. Nucl. Phys. **42**, 913 (1985) [Yad. Fiz. **42**, 1441 (1985)].
- [36] A. Palazzo, Phys. Rev. D **83**, 113013 (2011).
- [37] T. Kikuchi, H. Minakata, and S. Uchinami, J. High Energy Phys. 03 (2009) 114.